SCATTER RADIATION IN RADIOGRAPHY

Gerd-Ruediger JAENISCH, Uwe EWERT, and Mirko JECHOW

FEDERAL INSTITUTE FOR MATERIALS RESEARCH AND TESTING, Berlin, Germany

INTRODUCTION

In radiography, penetrating the object with X-rays and recording the transmitted radiation gives information about the inner structure of an object. The transmitted radiation consists of a primary and a scattered component. Textbooks on radiography consider the scattered radiation as unwanted due to radiation safety issues and the effect of contract reduction while carrying no information about the object. Additional it is stated, that, in practice, image unsharpness is given by inherent and geometrical unsharpness only while unsharpness due to the effect of scatter in the object is negligible. The paper presents theoretical and experimental investigations discussing the following effects in contact radiography: (i) scatter unsharpness and contrast is an issue to be considered; (ii) scattered radiation contributes to the image contrast, i.e. carries information about the object structure, depending on the size of the discontinuity, the radiation energy used, and the material of the object. The discussion becomes relevant for computed radiography (CR) as well as film radiography.

To evaluate the contribution of scattered radiation separated from the primary beam simulation has been applied. The Monte Carlo approach is capable to count for primary and secondary interaction mechanisms contributing to the image formation process like photon interactions (absorption, incoherent and coherent scattering including electron-binding effects, pair production, X-ray fluorescence) and electron interactions (electron tracing including X-Ray fluorescence and Bremsstrahlung production). It is a powerful tool to separate different influencing factors. This paper gives an overview about our Monte Carlo implementation McRay [1, 2] for radiation techniques. The major goal for this development is to handling complex geometries. The developed special Monte Carlo tracer allows calculating the photon path in CAD geometries with STL being the exchange format with industrial CAD packages. The results obtained from the Monte Carlo code have been verified by comparing with the MCNP code [3]. We show the comparison of our calculations with experimental results verifying the prediction of scatter unsharpness and scatter contrast.

X-RAY MODELLING BY MONTE CARLO RAY TRACER, COUPLED TO CAD OBJECT DESCRIPTION

Physics of Photon Transport

For the treatment of radiation techniques like radiography, only photon interactions are considered. The physics treatment for the photon transport presented here includes the photoelectric effect, coherent and incoherent scattering. Considering photon energies smaller then 1 MeV pair production does not occur. Additionally form factors and scattering functions are used with coherent and incoherent scattering to count for electron binding effects. Secondary effects like X-ray fluorescence and electron transport are neglected.

The stationary Bolzmann equation (1) is used to model the photon transport

$$\mathbf{\Omega} \cdot \nabla I(\mathbf{r}, E, \mathbf{\Omega}) + \mu(E) I(\mathbf{r}, E, \mathbf{\Omega}) = \int_0^\infty dE' \int_{4\pi} d\Omega' \, \sigma(E' \to E, \mathbf{\Omega}' \to \mathbf{\Omega}) I(\mathbf{r}, E', \mathbf{\Omega}'). \qquad (1)$$

It describes the variation of the photon flux $I(\mathbf{r}, E, \mathbf{\Omega})$ at position $\mathbf{r}$ with direction $\mathbf{\Omega}$ and energy E. The left hand side of Eq. (1) counts for the reduction of the flux by the interaction of photons with matter given by the linear attenuation coefficient $\mu(E)$ while the right hand side describes the increase of the photon flux $I(\mathbf{r}, E, \mathbf{\Omega})$ by scattering contributions from other energies E' and other directions $\mathbf{\Omega}'$ given by the scattering cross section $\sigma(E' \to E, \mathbf{\Omega}' \to \mathbf{\Omega})$. Internal photon sources such as X-ray fluorescence or Bremsstrahlung are neglected here.

The photoelectric effect is treated as a pure absorption of the photon which transfers its total energy to an electron in some shell of an atom. The energy of the photon can be sufficient to lift an electron from an inner to an outer shell or to remove the electron completely and to ionize the atom. As the energy of the photon increases absorption becomes possible by inner shell electrons. When the energy of the photon reaches the binding energy of a particular shell of electrons the absorption coefficient increases abruptly because more electrons are available for interaction. The energy at which this sharp increase occurs is called absorption edge, which is characteristic for every atom.

Scattering can be incoherent, which is known as Compton scattering, or coherent, which is called Rayleigh scattering. Whereas a photon transfers its total energy to an orbital electron while undergoing an absorption event, it loses no or only a part of its energy and is redirected if a scattering event occurs.

To model Compton scattering the angle of scattering θ and the new energy E' of the photon are determined. The analysis of the Compton process shows that the energy of the scattered photon E' is always less than that of the primary photon $E > E'$. The remaining energy is transferred to the struck electron as kinetic energy. The energy shift predicted depends only on the scattering angle θ and not on the nature of the scattering medium. The larger the scattering angle the larger the energy shift observed. The relationship between the scattering angle and the energy shift can be found from

the conservation of energy and momentum during the collision if assuming particle properties of the photon:

$$E' = \frac{E}{1 + \varepsilon(1 - \cos\theta)} \tag{2}$$

with $\varepsilon = E / m_0c^2 = E/511$ keV. The differential Compton scattering cross section is obtained from a combination of the Klein Nishina cross section σ_{KN} and non-relativistic Hartree-Fock incoherent scattering function $I(Z,E,\theta)$ [4] counting for electron binding effects

$$\sigma_{Compton} = I(Z,E,\theta) \cdot \sigma_{KN} \tag{3}$$

with the well know Klein Nishina formula giving the scattering cross section for a free electron

$$\sigma_{KN} = \frac{r_0^2}{2}\left\{\frac{1}{[1+\varepsilon(1-\cos\theta)]^2}\left[1+\cos^2\theta+\frac{\varepsilon^2(1-\cos\theta)^2}{1+\varepsilon(1-\cos\theta)}\right]\right\} \tag{4}$$

with the classical electron radius $r_0 = e^2/m_0c^2 = 2.818 \cdot 10^{-15}$ m (e - elementary charge, m_0 - rest mass of the electron, c – velocity of light in vacuum). The effect of $I(Z,E,\theta)$ is to decrease the Klein Nishina cross section in forward direction, for low energies E and high atomic numbers Z. For any Z the incoherent scattering function increases from zero to Z.

The coherent or Rayleigh scattering involves no energy loss of the photon upon being scattered by an atom. It is only a photon process that does not produce electrons for further transport. Only the scattering angle θ has to be computed and then the transport of the photon continues. The Rayleigh scattering cross section is obtained from the Thomson cross section $\sigma_{Thomson}$ and the relativistic Hartree-Fock atomic form factor $C(Z,E,\theta)$ [5] counting for electron binding effects

$$\sigma_{Rayleigh} = C^2(Z,E,\theta) \cdot \sigma_{Thomson} \tag{5}$$

with the Thomson formula giving the scattering cross section for a free electron which does not depend on the photon's energy and is equivalent to the Klein Nishina formula at zero energy

$$\sigma_{Thomson} = \frac{r_0^2}{2}(1+\cos^2\theta) = \sigma_{KN}(E=0). \tag{6}$$

The general effect of $C^2(Z,E,\theta)$ is to decrease the Thomson cross section for backward scattering, and to strongly increase the Thomson cross section in forward direction. This effect is opposite in these respects to the effect of the scattering function $I(Z,E,\theta)$ on the Klein Nishina cross section in Compton scattering. For a given Z the form factor decreases from Z to zero. Note that for high energies, coherent scattering virtually occurs only in forward direction within a very small angle range. From a transport point of view it appears that no scattering took place. Consequently, it contributes much greater if electron binding effects are considered. In general, Rayleigh scattering

occurs only for soft radiation for which the binding energy of the electrons in their atomic shell is important. It is most important for elements of high atomic number and low photon energies.

Monte Carlo Model

The following assumptions are made to formulate the Monte Carlo model of photon transport: (*i*) the particles travel on a straight path between two interaction events without energy loss, (*ii*) one interaction per unit length occurs given by the linear attenuation cross section μ, (*iii*) the duration of an interaction is negligible compared to the time between two interactions. For photon transport three independent and mutually exclusive random events are considered: absorption τ, Compton scattering $\sigma_{Compton}$, and Rayleigh scattering $\sigma_{Rayleigh}$. The probability p_i of the collision event i is given by the ratio of the interaction cross section of the event i and the linear attenuation cross section μ: $p_1 = \tau / \mu$, $p_2 = \sigma_{Compton} / \mu$, $p_3 = \sigma_{Rayleigh} / \mu$.

The attenuation law determines the collision length l of a photon. Assuming piecewise constant material parameters the collision length is given by

$$l = -\frac{\ln \xi}{\mu} \tag{7}$$

with $\xi \in [0,1]$ being a uniformly distributed random number.

The implemented transport scheme consists of the three standard elements of Monte Carlo techniques: determination of (*i*) initial condition $(E_0, \mathbf{\Omega}_0)$, (*ii*) location of interaction from collision length l, and (*iii*) collision event i. If the photon leaves the object no more interaction events are considered and the realization is terminated after registration in a detector element if hit. In case of an absorption event the realization is likewise finished. For a scattering event follows the determination of the new flight path direction and a possible energy loss $(E, \mathbf{\Omega}) \to (E', \mathbf{\Omega}')$, after which the scheme is repeated for the same realization from the second step until termination. The scheme is repeated until the preset number of realizations is traced or the required statistical accuracy is reached.

Object Description

In addition to the model of radiation transport, the radiographic simulation requires a virtual representation of the part or construction under testing. Unlike other Monte Carlo codes such as MCNP [3], an interface to CAD has been realized. Objects are described by closed surfaces separating regions of homogeneous material described by its attenuation properties. Several objects can be arranged in a virtual scene combined by simple Boolean operators forming complex parts. This realization also allows a flexible flaw generation and arbitrary positioning of flaws in complex parts.

The surface of an object is described by plane polygons allowing a simple mathematical treatment of a single polygon or facet. The size of the polygons is given by the local surface curvature and the

required accuracy of the surface approximation. The STL (stereo lithography) data format is used as exchange format for surfaces representation by triangles.

Monte Carlo Tracer

Primary and scattered photons are treated independently. The contribution of primary photons is calculated analytically from the attenuation law

$$I_p\left(\boldsymbol{r},\boldsymbol{\Omega},E\right) = I_0\left(\boldsymbol{r},\boldsymbol{\Omega},E\right)e^{-\int_0^{|r-r_0|}\mathrm{d}R\,\mu(r-R\boldsymbol{\Omega},E)}. \tag{8}$$

Accordingly, only the scattered photons are traced by the Monte Carlo method. The probability for a surviving photon is given by $p_s = \mu_S/\mu$ with $\mu_S = \sigma_{Compton} + \sigma_{Rayleigh}$. This weight describes the average fraction of photons, which did not experience an absorption event. Accordingly, the surviving probability of a photon being scattered n-times follows as

$$p_s\left(n+1\right) = p_s\left(n\right)\frac{\mu_s\left(n+1\right)}{\mu\left(n+1\right)}. \tag{9}$$

This photon is registered with the weight given by eq. (9) at the detector plane if hit by elongating its path. It can formally be interpreted as an increase of the number of photon sources compared to the standard direct tracing of the photon's trajectory. Every following collision or scattering event decreases the photon weight and therefore its contribution to the final result. This treatment yields a reduction of variance in the result.

The described Monte Carlo algorithm has been implemented for parallel processing using MPI. The calculations presented here have been performed using 100 processors and a total number of photons traced of $1\cdot10^9$ (0.5 mm pixel size) and $1\cdot10^{11}$ (0.04 mm pixel size) resulting in statistical error for the scattered distribution of about 0.02 per pixel. The distance between the radiation source and the detector is 1000 mm assuming a monochromatic point source emitting photons at energy of 100 keV. The distance between the object and the detector has been chosen to be 0 mm, 5 mm, and 55 mm. As detector an ideal photon counter has been used.

RESULTS OF MODELLING FOR NOTCH PLATES AND ITS VERIFICATION

Radiographs of different notch plates were calculated. A real notch plate was manufactured with notches of 0.03 mm to 2 mm width varying in depth from 0 to 3 mm (see Figure 1). The notch plate is made from steel and was used to verify the modelling data.

Scatter Contrast and Scatter Unsharpness

In most textbooks radiographic image quality parameters are restricted to contrast, noise (or granularity) and unsharpness. The scatter contribution is typically explained by the build up factor B_{up} which considers the scatter ratio k as quotient of intensity of scattered radiation I_s to primary radiation I_p (see also ASTM E1000) with:

$$B_{up} = 1 + \frac{I_s}{I_p} = 1 + k. \tag{10}$$

The simplified attenuation law is given by:

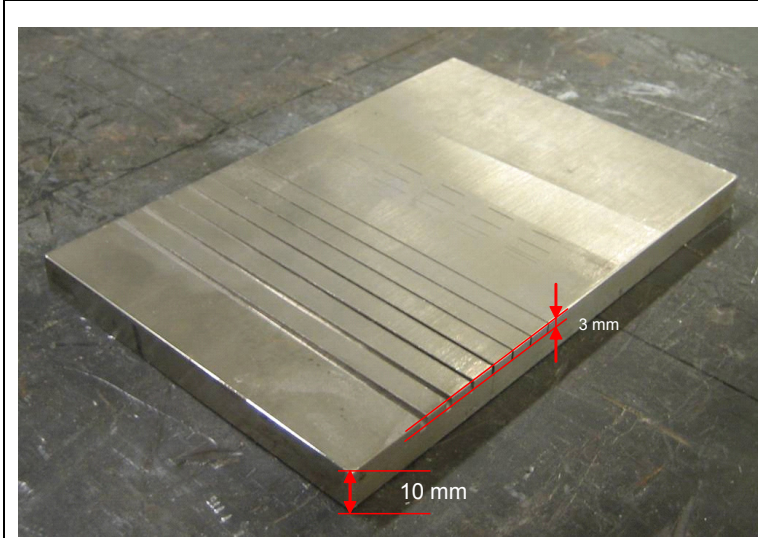$$I = I_0 \cdot e^{-\mu \cdot w} \cdot B_{up}. \tag{11}$$
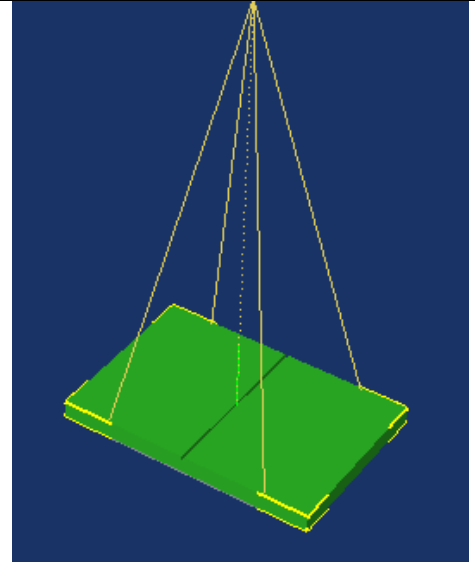

| Figure 1a. Notch plate of steel. | Figure 1b. CAD-model of notch plate. |

The modelling software allows the separate calculation of primary radiation and scattered radiation. The goal of the study was the quantitative determination of the contribution of the scattered radiation. The results show a significant contrast enhancement due scattered radiation which depends on the notch width. The scatter image contributes with additional scatter unsharpness. Figure 2 shows the separated profiles generated by primary and scattered radiation for a detector in contact to the notch plate. The scatter image contributes to the wider notches with about 30% of the total image contrast. The contrast enhancement depends on the notch width and decreases with decreasing width of the notches. This effect leads to a variation of the radiation intensity behind notches of the same depth without any unsharpness contribution of the detector and geometrical unsharpness. The contrast of the fine flaws is reduced in relation to the larger ones, which has to be considered if digital tools are used to determine the flaw depth on the basis of a μ calibration at large flaws, step wedges, flat bottom holes or plate IQIs.

The notch plate (Figure 1a) was used for verification of the modelling results. An imaging plate HD-IP and an IP scanner HD-CR 35 NDT of Duerr was used as detector. The imaging plate (IP) was protected by a flexible polyethylene envelope without lead screens. All measurements were performed with a constant potential X-ray tube, Rich. Seifert & Co, AEG MB 450/1 (7 mm Be-Window), at 160 kV. The notch plate and IP was exactly positioned in 4 m distance to the x-ray

tube to neglect the geometrical unsharpness. The IP was scanned with 21 μm pixel resolution of the Duerr scanner.
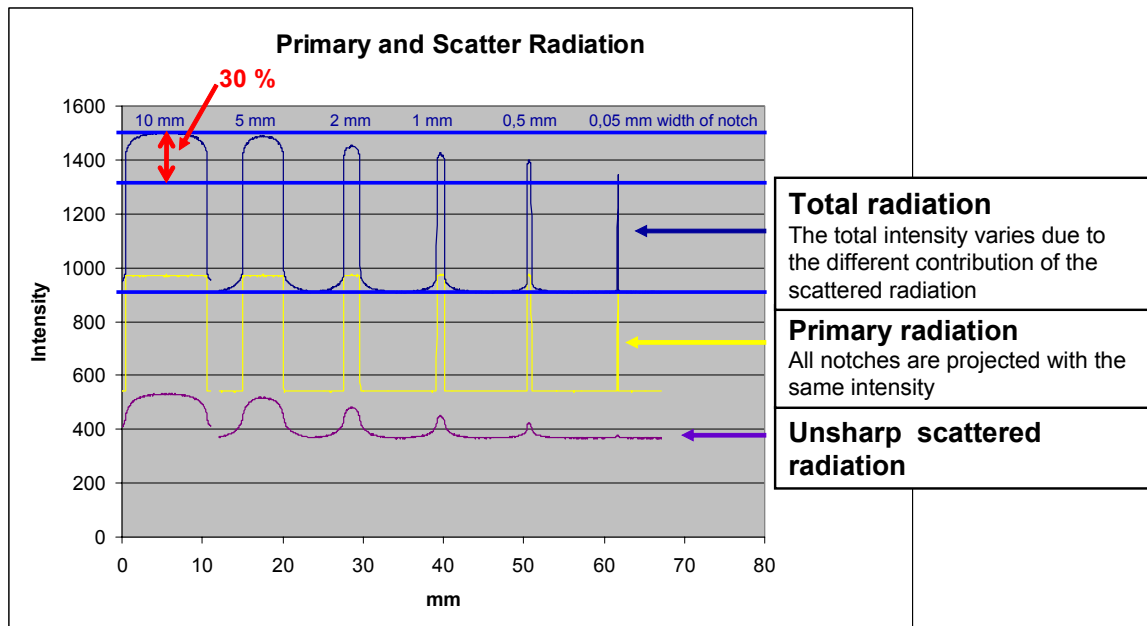

Figure 2. Profiles of calculated contributions from scattered and primary radiation. The scattered radiation enhances the total contrast by about 30% for the wide notches and is negligible for the finest notches. Calculation for a 10 mm thick steel plate and 2 mm notch depth.

Figure 3 shows the comparison of measured and calculated data. The unsharpness is visible in the curvature of the foot areas and as arc like shape in the top area of the notch profiles. The experimental and calculated data show sufficient agreement after normalisation to consider the IP sensitivity. The comparison was carried out for the 2 mm deep notch with 2 mm, 1 mm, and 0.5 mm width. Fine notches with a width below 0.05 mm are not significantly enhanced by the scatter contrast. This means they appear in the radiograph with about 30% less contrast in comparison to the large flaws.

The effect of additional scatter contrast and unsharpness depends on the distance between detector and object (see Figure 4). This effect was studied by modelling. The detector was located in contact with the notch plate as well as in 5 mm and 55 mm distance to the plate. The distance between detector and object is typical for radioscopy, the usage of digital detector arrays (DDA) and computed tomography. A DDA is typically used in some distance to the object due to the dimension of the detector casing and for protection of the detector. Films and imaging plates are used in dependence on the cassette size in contact or in few mm distance, respectively. The observed change of scatter contrast has to be considered for the determination of the exposure time. For 5 mm and 55 mm distance a Hamamatsu C7940DA-02 was carefully positioned and calibrated. A multi

gain calibration was used to achieve the high contrast sensitivity mode, which was described earlier [5]. Figure 4 shows the comparison between calculations and measurements. The experimental data were normalised differently to correct for the different sensitivity of DDA and IP.
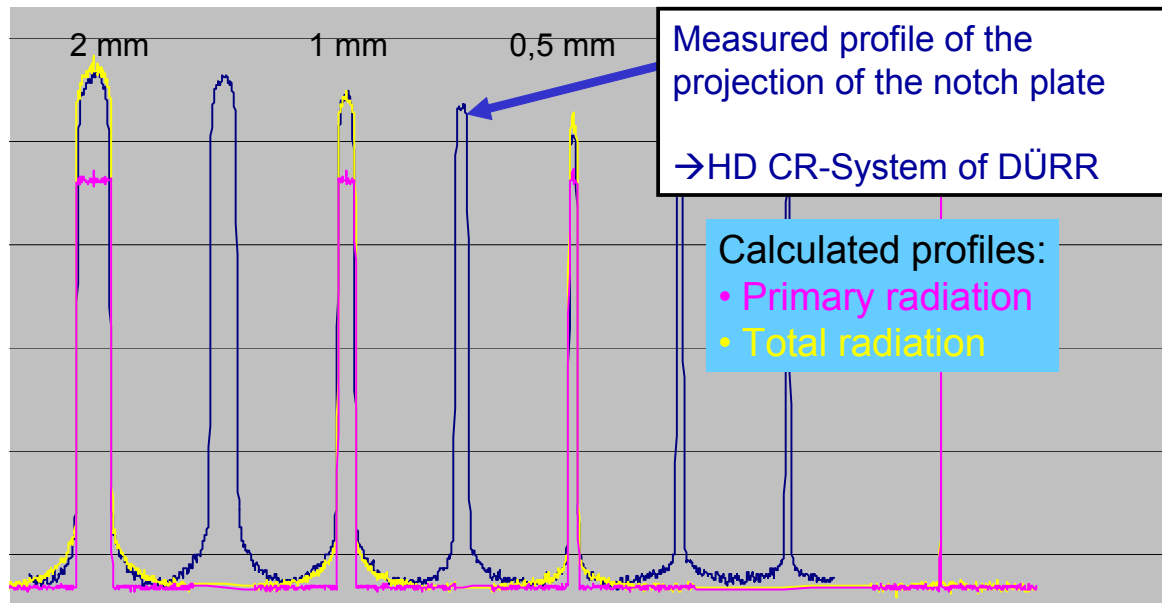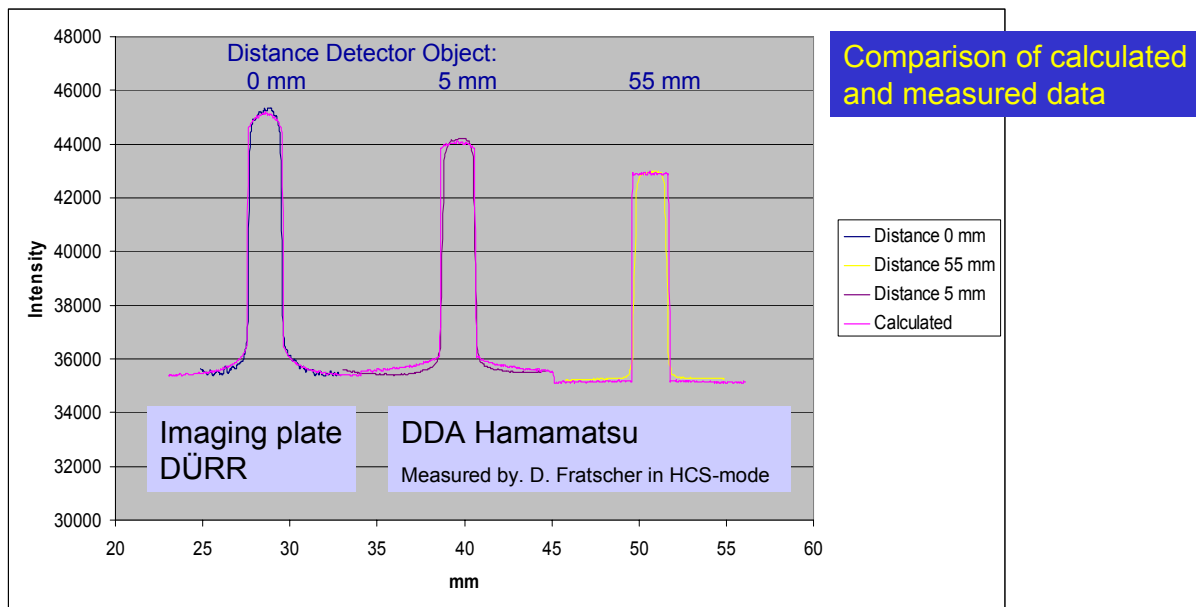

Figure 3. Comparison of calculated and measured profiles of the notch plate for 2 mm, 1 mm and 0.5 mm wide and 2 mm deep notches.

Figure 4. Contrast and unsharpness reduction of calculated and measured notch profiles in different distances of the notch plate from the detector. The contrast varies by 20 %.

CONCLUSIONS

State-of-the-art radiography simulators have a broad application range. These simulators are based on the attenuation law to describe the primary radiation. Monte Carlo models can be used to describe the effect of scattered radiation in detail. The discussed Monte Carlo implementation overcomes the problem of standard codes in handling complex part geometries because it couples Monte Carlo photon transport with CAD object description.

Monte Carlo simulations were conducted to separate the contributions of primary and scattered radiation for a notch plate of steel to the total radiographic image. The scattered radiation generates an additional image, which is overlapped with the primary radiation image. The scatter image is unsharp and therefore the total image is characterised by a scatter unsharpness too. The simulated radiographs were successfully verified with real exposures of imaging plates and a DDA.

REFERENCES

1. M. Zhukovskiy, S. Podoliako, G.-R. Tillack, and C. Bellon, "Monte Carlo Simulation of Photon Transport Coupled to CAD Object Description." In: D. O. Thompson and D. Chimenti (Eds.): Review of Progress in Quantitative Nondestructive Evaluation, Vol. 23, AIP, Melville, 2004, pp. 515-521.

2. V. Zagonov, M. Zhukovskiy, S. Podoliako, M. Skatchkov, G.-R. Jaenisch, and C. Bellon, "Application of Boundary Oriented Object Description for the Simulation of Transport of Ionizing Radiation for Computed Diagnostics." (in Russian). Mathematical Modelling **16** 5, 103-116 (2004)

3. Briesmeister, J. F. (ed.), "MCNP–A General Monte Carlo N–Particle Transport Code." LANL Report LA–13709–M, Los Alamos, 2000

4. J. H. Hubbell, W. J. Veigele, E. A. Briggs, R. T. Brown, D. T. Cromer, and R. J. Howerton, "Atomic Form Factors, Incoherent Scattering Functions, and Photon Scattering Cross Sections." J. Phys. Chem. Ref. Data **4,** 471-538 (1975); erratum in **6,** 615-616 (1977)

5. J. H. Hubbell and Overbo, "Relativistic Atomic Form Factors and Photon Coherent Scattering Cross Sections." J. Phys. Chem. Ref. Data **8,** 69-105, (1979)

6. U. Ewert, U. Zscherpel, K. Bavendiek. „Replacement of Film Radiography by Digital Techniques and Enhancement of image Quality." Proceedings of the Annual Conference of Indian NDT society, Kalkutta, 4.-6.12.2005, V.S. Jain-Lecture, pp. 3-15.